Mn2+ Complexes Containing Sulfonamide Groups with pH-Responsive Relaxivity

Rocío Uzal-Varela, Aurora Rodríguez-Rodríguez, Miguel Martínez-Calvo, Fabio Carniato, Daniela Lalli, David Esteban-Gómez, Isabel Brandariz, Paulo Pérez-Lourido, Mauro Botta, and Carlos Platas-Iglesias

Inorganic Chemistry 2020 59 (19), 14306-14317
DOI: 10.1021/acs.inorgchem.0c02098

Mn^{2+} Complexes Containing Sulfonamide Groups with pH-Responsive Relaxivity

Rocío Uzal-Varela,[†] Aurora Rodríguez-Rodríguez,[†] Miguel Martínez-Calvo,[†] Fabio Carniato,[‡] Daniela Lalli,[‡] David Esteban-Gómez,[†] Isabel Brandariz,[†] Paulo Pérez-Lourido,[§] Mauro Botta,*[,‡] and Carlos Platas-Iglesias*[,†]

[†] Centro de Investigacións Científicas Avanzadas (CICA) and Departamento de Química Fundamental, Universidade da Coruña, Campus da Zapateira-Rúa da Fraga 10, 15008 A Coruña, Spain

[‡] Dipartimento di Scienze e Innovazione Tecnologica, Università del Piemonte Orientale "A. Avogadro", Viale T. Michel 11, 15121 Alessandria, Italy.

[§] Departamento de Química Inorgánica, Facultad de Ciencias, Universidade de Vigo, As Lagoas, Marcosende, 36310 Pontevedra, Spain

ABSTRACT: We present two ligands containing a *N*-ethyl-4-(trifluoromethyl)benzenesulfonamide group attached to either a 6,6'-(azanediylbis(methylene))dipicolinic acid unit (H_3DPASAm) or a 2,2'-(1,4,7-triazonane-1,4-diyl)diacetic acid macrocyclic platform (H_3NO2ASAm). These ligands were designed to provide pH-dependent relaxivity response upon complexation with Mn^{2+} in aqueous solution. The protonation constants of the ligands and the stability constants of the Mn^{2+} complexes were determined using potentiometric titrations complemented by spectrophotometric experiments. The deprotonation of the sulfonamide groups of the ligands are characterized by protonation constants of $\log K_i^H$ = 10.36 and 10.59 for $DPASAm^{3-}$ and $HNO2ASAm^{2-}$, respectively. These values decrease dramatically to $\log K_i^H$ = 6.43 and 5.42 in the presence of Mn^{2+} due to the coordination of the negatively charged sulfonamide groups to the metal ion. The higher $\log K_i^H$ value in $[Mn(DPASAm)]^-$ is related to the formation of a seven-coordinate complex, while the metal ion in $[Mn(NO2ASAm)]^-$ is six-coordinated. The X-ray crystal structure of $Na[Mn(DPASAm)(H_2O)]\cdot 2H_2O$ confirms the formation of a seven-coordinate complex, where the coordination environment is fulfilled by the donor atoms of the two picolinate groups, the amine N atom, the N atom of the sulfonamide group and a coordinated water molecule. The lower conditional stability of the $[Mn(NO2ASAm)]^-$ complex and the lower protonation constant of the sulfonamide group results in complex dissociation at relatively high pH (< 7.0). However, protonation of the sulfonamide group in $[Mn(DPASAm)]^-$ falls into the physiologically relevant pH window and causes a significant increase in relaxivity from r_{1p} = 3.8 mM^{-1} s^{-1} at pH 9.0 to r_{1p} = 8.9 mM^{-1} s^{-1} at pH 4.0 (10 MHz, 25 ºC).

INTRODUCTION

Contrast agents for application in Magnetic Resonance Imaging (MRI) are a class of paramagnetic compounds that are injected in the body to enhance image contrast and thus aid a more precise and accurate diagnosis of different pathologies.[1,2] Paramagnetic ions containing Mn^{2+} and Fe^{3+} were considered as MRI agents in the early times of MRI, back in the 1970s and early 1980s.[3-6] Soon after it was discovered that some Gd^{3+} complexes are very efficient relaxation agents,[7] which were subsequently introduced in clinical practice and applied to aid diagnosis in millions MRI scans every year.[1] Contrast agents based on Gd^{3+} are complexes with polyaminopolycarboxylate ligands that ensure a very high stability to avoid the release of the toxic metal ion in vivo.[8] These complexes contain a water molecule coordinated to the metal ion that exchanges with the water of the surrounding tissues, providing an efficient mechanism to shorten the relaxation times of water proton nuclei and thus increase the signal intensity.[9]

The contrast agents available in the market are considered very safe pharmaceuticals, though some problems of toxicity were reported. These toxicity issues have been associated with the administration of Gd^{3+} agents to patients having renal impairment, which accumulate the metal ion in the body and in some cases develop a potentially fatal disease called nephrogenic systemic fibrosis.[10,11] This prompted the different medicine agencies to revise some of the protocols and prescribe information warnings, which prevented the detection of new cases. More recently, reports of Gd^{3+} deposition in the brain and other organs opened the debate on the long-term safety of some Gd^{3+} contrast agents,[12] which eventually led to the suspension of the authorizations in Europe of some of the agents based on non-macrocyclic structures.[13]

The last decade witnessed a renewed interest in developing transition-based MRI probes as alternatives to the classical Gd^{3+}

agents.[14,15] In particular, both Mn^{2+} and Fe^{3+} complexes were proposed as Gd^{3+} alternatives as T_1-shortening contrast agents, as they can reach relaxivities comparable to those of commercially available Gd^{3+} agents.[16,17] These two metal ions present ^6S ground energy terms for the free ion, that often originate ground energy electronic states characterized by slow relaxation times of the electron spin in high-spin complexes, making them powerful relaxation agents. As in the case of Gd^{3+} agents,[18-20] responsive contrast agents may be designed by programming a change in the number of coordinated water molecules triggered by an alteration of a physiologically relevant parameter (i. e. pH, concentration of biogenic anions or cations). This was demonstrated recently by Tircsó et al. with the [Mn(PC2A-EA)] complex (Chart 1). The aminoethyl group of the ligand is protonated in the biologically relevant pH window ($\log K_{MnL}^{H} = 6.88$), so that a water molecule replaces the amine donor atom, causing a remarkable relaxivity increase.[21]

Chart 1. Ligands discussed in the present work.

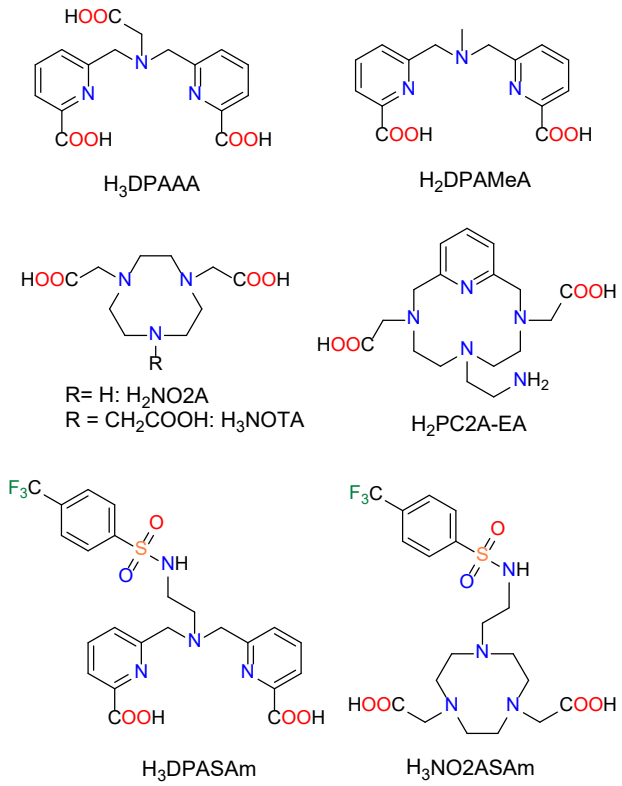

A few years ago, we initiated a research program aiming to develop potential candidates as Mn^{2+}-based MRI contrast agents. We developed a series of ligands based on both macrocyclic and acyclic frameworks, functionalized with picolinate or acetate pendant arms. Some representative members of the picolinate family are H_3DPAAA, H_2DPAMeA and their derivatives (Chart 1).[22,23] Among the macrocyclic ligands, we explored derivatives of 1,4,7,-tetraazacyclononate,[24] for instance containing two acetate groups (H_2NO2A) incorporating different functions on the third N atom of the macrocyclic unit,[25] or cyclen-based ligands like H_2DO2A and related systems.[26] The Mn^{2+} complexes of $DPAAA^{3-}$ and $NO2A^{2-}$ were shown to contain a water molecule coordinated to the metal ion, DPAMeA yields a Mn^{2+} complex with two inner-sphere water molecules.

The *N*-ethylbenzenesulfonamide group was found to be well suited to provide Gd^{3+}-based agents with pH-dependent modulation of ^1H relaxivity.[27] Thus, we hypothesized that the incorporation of an *N*-ethylbenzenesulfonamide group to these platforms should provide rather stable Mn^{2+} complexes with pH-responsiveness, as the deprotonated sulfonamide group is expected to remain coordinated to the metal ion. Sulfonamide protonation should trigger the coordination of a water molecule replacing the sulfonamide N atom, resulting in an increase of proton relaxivity and thus MRI contrast.

Herein, we present the synthesis and characterization of the ligands containing *N*-ethyl-4-(trifluoromethyl)benzenesulfonamide groups H_3DPASAm and H_3NO2ASAm (Chart 1). The presence of the electron-withdrawing CF_3 group was envisaged to push the pK_a of the sulfonamide group to the biologically relevant window, in view of the lower charge of Mn^{2+} compared to Gd^{3+}. We report the synthesis of the ligands, a detailed assessment of the thermodynamic stability of the corresponding Mn^{2+} complexes and their relaxometric behavior. We also present the X-ray structure of the $[Mn(H_3DPASAm)]^-$ complex.

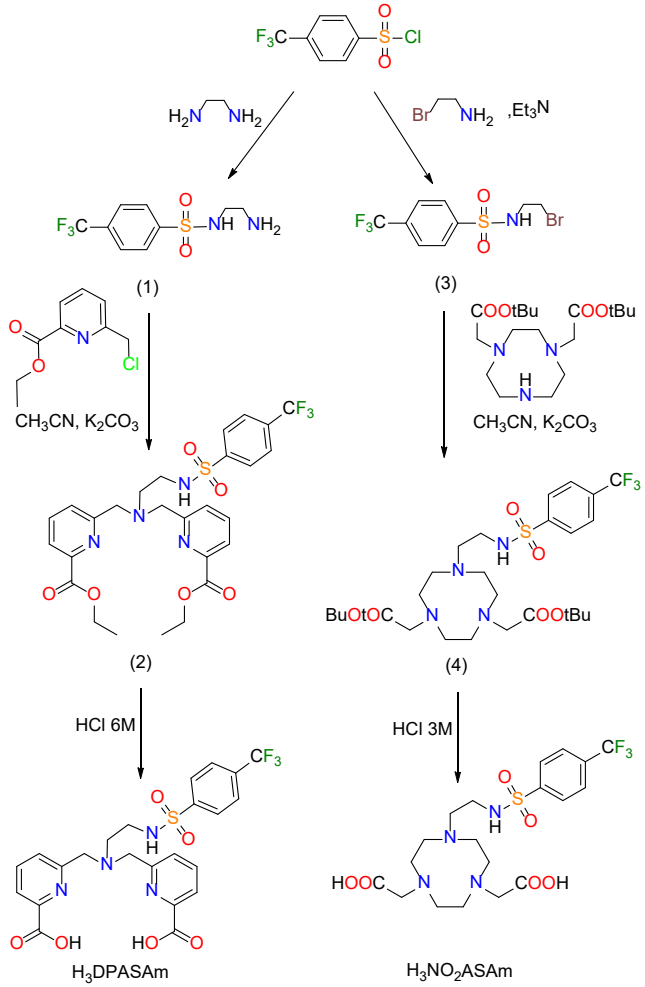

Scheme 1. Synthesis of the H_3DPASAm and NO2A(O^{t}Bu)$_2$ ligands.

RESULTS AND DISCUSSION

Synthesis. The H_3DPASAm ligand was synthesized by alkylation of *N*-(2-aminoethyl)-4-(trifluoromethyl)benzenesulfonamide (**1**) with ethyl 6-(chloromethyl)picolinate and subsequent acid hydrolysis of the ester groups (Scheme 1). Compound **1** was obtained in 92% by reaction of 4-(trifluoromethyl)benzenesulfonyl chloride and ethylendiamine in CH_2Cl_2 at 0 ºC. The ligand was isolated with an overall yield of 36% over the three steps. Ligand H_3NO2ASAm was prepared by alkylation of the NO2A(O^tBu)$_2$ precursor with *N*-(2-bromoethyl)-4-(trifluoromethyl)benzenesulfonamide (**3**) in acetonitrile in the presence of K_2CO_3 as a base (Scheme 1). The latter was isolated in 81% yield by reaction of 2-bromoethan-1-amine hydrobromide and 4-(trifluoromethyl)benzene sulfonyl chloride using Et_3N as a base. Acid hydrolysis of the *tert*-butyl ester groups of the ester intermediates **4** with 3 M HCl at room temperature afforded the desired ligand in 71% yield over the three steps.

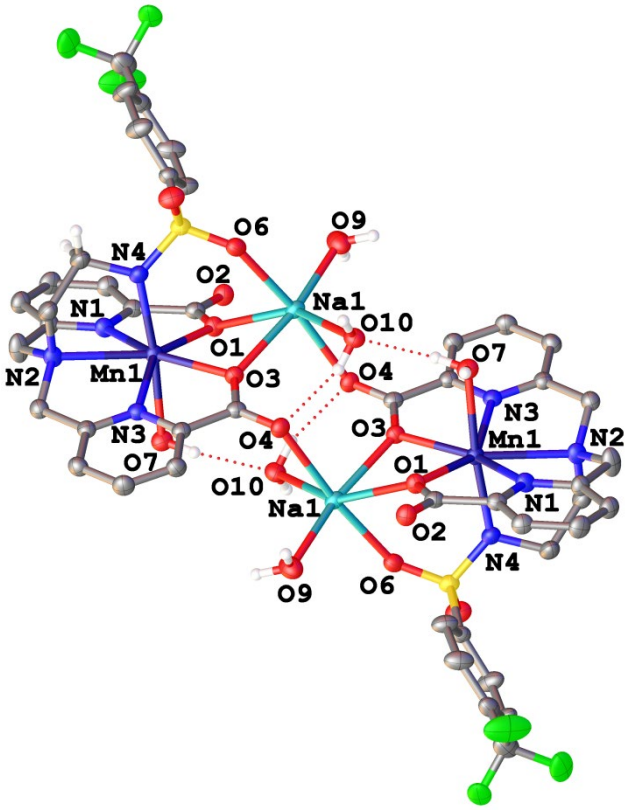

Figure 1. X-ray crystal structure of Na[Mn(DPASAm)(H_2O)]·2H_2O with atom numbering. The ORTEP plot is at the 50% probability level.

X-ray structures. Single crystals with formula Na[Mn(DPASAm)(H_2O)]·2H_2O were obtained by slow evaporation of an aqueous solution of the complex at pH 9.9. Crystals contain two [Mn(DPASAm)(H_2O)]$^-$ complexes joined by two Na^+ cations, generating a centrosymmetric {Na_2(H_2O)$_2$[Mn(DPASAm)(H_2O)]$_2$} entity (Figure 1). Table 1 presents the bond distances of the metal coordination environments. Each Mn^{2+} ion is coordinated to the tertiary N atom of the ligand N2 and the donor atoms of the picolinate groups N1, N3, O1 and O3, which define a pentagonal plane of the pentagonal bipyramidal coordination polyhedron (deviation from planarity 0.19 Å). Heptacoordination is relatively rare in first-row transition metal complexes, being however more common for Mn than for any other element of the series.[28] The nitrogen atom of the sulfonamide group N4 and the oxygen atom of a coordinated water molecule O7 occupy the apical positions of the pentagonal bipyramid. The N4-Mn1-O7 angle (174.76(8)º) deviates by ~5º from the linear value expected for a pentagonal bipyramid. The angles defined by adjacent donor atoms of the equatorial plane and the metal ion fall within the range 68.8 – 79.3º, and thus present relatively small deviations from the ideal value (72º).

The sulfonamide N atom N4 gives the strongest interaction with the Mn^{2+} ion, while the tertiary amine N atom N2 appears to provide a rather weak bond, as usually observed in complexes with tripodal ligands.[29] The bond distances involving the donor atoms of the picolinate groups are similar to those reported for related seven-coordinate Mn^{2+} complexes.[24,29] The sulfonamide group is a relatively common motif in Mn^{2+} coordination chemistry that is generally coordinated through the N atom.[30]

The Na^+ cations are coordinated to an oxygen atom of the sulfonamide group (O6) and three oxygen atoms of the carboxylate groups (O1, O3 and O4). The carboxylate group containing O1 and O4 is involved in μ^3-η^1:η^2 coordination through O1 and O4, while the carboxylate group containing O3 provides a μ^2-η^2 coordination.[31] Six-coordination is completed by the oxygen atoms of two water molecules, resulting in a distorted octahedral environment around the Na^+ cations. The Mn-O distance involving the μ^2-η^2 carboxylate (Mn-O3 = 2.2188(15) Å) is ca. 0.05 Å shorter than the Mn-O1 bond (2.2600(15) Å), which implies a μ^3-η^1:η^2 carboxylate.

Table 1. Bond distances (Å) of the metal coordination environments in Na[Mn(DPASAm)(H_2O)]·2H_2O.

Mn1-N4	2.197(2)	Na1-O1	2.5295(18)
Mn1-O3	2.2188(15)	Na1-O3	2.3951(17)
Mn1-O1	2.2600(15)	Na1-O4	2.4741(18)
Mn1-N1	2.2609(19)	Na1-O6	2.3484(18)
Mn1-N3	2.2716(18)	Na1-O9	2.381(2)
Mn1-O7	2.3457(16)	Na1-O10	2.5160(18)
Mn1-N2	2.514(2)		

Ligand protonation constants and stability constants of the Mn^{2+} complexes. The protonation constants of the NO2ASAm^{3-} ligand were determined by potentiometric titrations at 25 ºC in 0.15 M NaCl. However, potentiometry did not allow an accurate determination of the values of logK_1^H and logK_2^H, likely because of partial (non-visible) precipitation of the ligand. Thus, both potentiometric and spectrophotometric titrations were used for independent protonation constant determination. Representative potentiometric titrations curves are presented in Figures S1-S2, Supporting Information. The protonation constants of DPASAm^{3-} were determined using spectrophotometric titrations, as precipitation was observed at the concentration required for potentiometric experiments (> 1 mM). Table 2 compares the determined logK_i^H values with those reported for the analogous ligands containing an acetate group replacing the sulfonamide pendant (DPAAA^{3-} and NOTA^{3-}).[22,32,33] The data reported in the literature for NOTA^{3-} was measured using 0.1 M ionic strengths, and thus we

used potentiometry to determine the protonation constants of this ligand using a 0.15 M NaCl background electrolyte.

The absorption spectrum of $DPASAm^{3-}$ recorded at pH = 0.82 is dominated by a band with a maximum at 269 nm, characteristic of the picolinic acid chromophore (Figure 2).[34] Increasing the pH causes an increase in the intensity of the absorption maximum, which experiences a slight shift to longer wavelengths. The absorption spectra recorded in the pH range 0.82-12.45 were fitted to obtain the ligand protonation constants listed in Table 2. The absorption spectra calculated for the different species present in solution are shown in Figure S3 (Supporting Information).

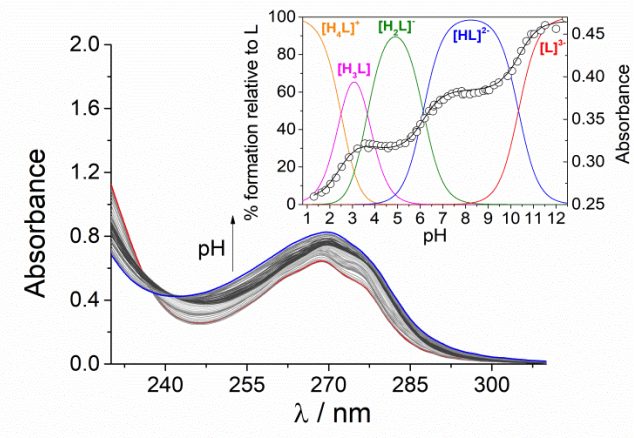

Figure 2. Absorption spectra of a 6.55×10^{-5} M solution of $DPASAm^{3-}$ recorded at different pH values (blue trace, pH = 12.45; red trace, pH = 0.82). Inset: Changes in absorbance at 249 nm (blue squares), fitted values (black line) and species distribution diagram.

The first protonation constant of the $DPASAm^{3-}$ ligand ($\log K_1^H$ = 10.36) can be assigned to the protonation of the sulfonamide N atom by comparison with the protonation constants of $DPAAA^{3-}$. This protonation constant is similar to that reported for DO3A ligands containing sulfonamide ($\log K^H$ = 11.02)[35] or dansyl ($\log K^H$ = 10.8)[36] groups. The second protonation event involves the amine N atom of the ligand, while $\log K_3^H$ and $\log K_4^H$ are associated with the protonation of the carboxylate functions of the picolinate groups.[37]

The $NO2ASAm^{3-}$ ligand presents two protonation constants with $\log K_i^H$ values of 11.26 and 10.59 that are related to the protonation of the sulfonamide group and a N atom of the macrocyclic fragment. However, an unambiguous attribution of each protonation event is not possible based on potentiometric data. We therefore performed spectrophotometric titrations in the pH range ca. 9-13. The absorption spectrum of the ligand recorded at pH ~ 9 presents a well-defined maximum at 268 nm with two additional components at 262 and 276 nm (Figure S4, Supporting Information), typical of the sulfonamide chromophore.[38] The increase in the pH of the solution provokes an increase of the intensity of the band, which becomes broader and ill defined. The absorption band experiences drastic changes above pH ~9, associated with a protonation constant of $\log K_2^H$ = 10.59(8). However, the protonation event associated with a protonation constant of $\log K_1^H$ = 11.26(7) is characterized by slight changes of the absorption spectrum. Thus, the first protonation constant of $NO2ASAm^{3-}$ can be attributed to the macrocyclic ring, while the second is assigned to the sulfonamide group. Therefore, the sulfonamide groups in $DPASAm^{3-}$ and $NO2ASAm^{3-}$ are characterized by very similar protonation constants. Spectrophotometric titrations of $NO2ASAm^{3-}$ in the pH range 1.6 to 6.2 were also performed (Figure S5, Supporting Information). Though spectral variations were not as pronounced as at basic pH, the protonation constants $\log K_3^H$ and $\log K_4^H$ obtained by this method show an excellent agreement with the potentiometric data (Table 2).

A comparison of the protonation constants associated with the amine N atom of $DPAAA^{3-}$ ($\log K_1^H$ = 7.26) and $DPASAm^{3-}$ ($\log K_2^H$ = 6.13) shows that the substitution of the acetate group by a N-ethylsulfonamide pendant causes a decrease of the basicity of the amine N atom. A similar effect is evident by comparing the $\log K_1^H$ values determined for $NO2ASAm^{3-}$ and $NOTA^{3-}$.

The first protonation constant determined for $NOTA^{3-}$ in 0.15 M NaCl is ca. 1 log*K* unit lower than that measured in 0.1 M Me_4NCl,[32] which likely reflects the formation of a relatively stable Na^+ complex. The remaining protonation constants determined using these two ionic strength backgrounds are in excellent agreement. Speciation diagrams calculated for $DPASAm^{3-}$, $NO2ASAm^{3-}$ and $NOTA^{3-}$ are presented in Figures S6-S8 (Supporting Information).

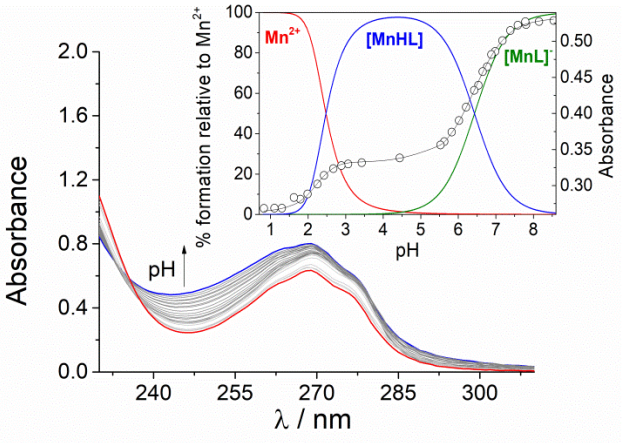

Figure 3. Absorption spectra of a 6.55×10^{-5} M solution of $DPASAm^{3-}$ and one equivalent of Mn^{2+} recorded at different pH values (blue trace, pH = 8.54; red trace, pH = 0.82). Inset: Changes in absorbance at 250 nm (blue diamonds) and species distribution diagram.

Table 2. Protonation constants of the ligands and stability constants of their Mn^{2+} complexes determined by potentiometric and spectrophotometric titrations at 25 ºC in 0.15 M NaCl.

	DPASAm^{3-} [b]	DPAAA^{3-} [a]	NO2ASAm^{3-}	NOTA^{3-} (I = 0.15 M)	NOTA^{3-} (I = 0.1 M)
logK_1^H	10.36(1)	7.26	11.26(7) [b]	12.05(6)	13.17[c] / 11.41[d]
logK_2^H	6.13(1)	3.90	10.59(8)[b]	5.77(6)	5.74 [c] / 5.74[d]
logK_3^H	3.68(1)	3.29	4.57(5) /4.57(5)[b]	3.30(6)	3.22 [c] / 3.16[d]
logK_4^H	2.43(1)	1.77	2.65(5) /2.69(5)[b]	2.20(7)	1.96 [c] / 1.71[d]
logK_{MnL}	13.53(1)	13.19	15.29(5)	15.6(1)	16.30 [c] /14.9 [e]
logK_{MnLH}	6.44(2)	2.90	5.52(5)		
logK_{MnLOH}	-	11.97			
pMn[f]	7.82	8.98	6.63	7.97	

[a] Equilibrium constants in 0.15 M NaCl and 25 ºC from reference 22. [b] Values obtained with spectrophotometric titrations at 25 ºC in 0.15 M NaCl. [c] Equilibrium constants in 0.1 M Me_4NCl ionic strength and 25 ºC from reference 32. [d] Equilibrium constants in 0.1 M ionic strength and 25 ºC from reference 33. [e] Stability constant in 0.1 M Me_4NCl ionic strength and 25 ºC from reference 39. [f] Defined as -log$[Mn^{2+}]_{free}$ at pH = 7.4 for $[Mn^{2+}]_{tot} = [L]_{tot} = 10^{-5}$ M.

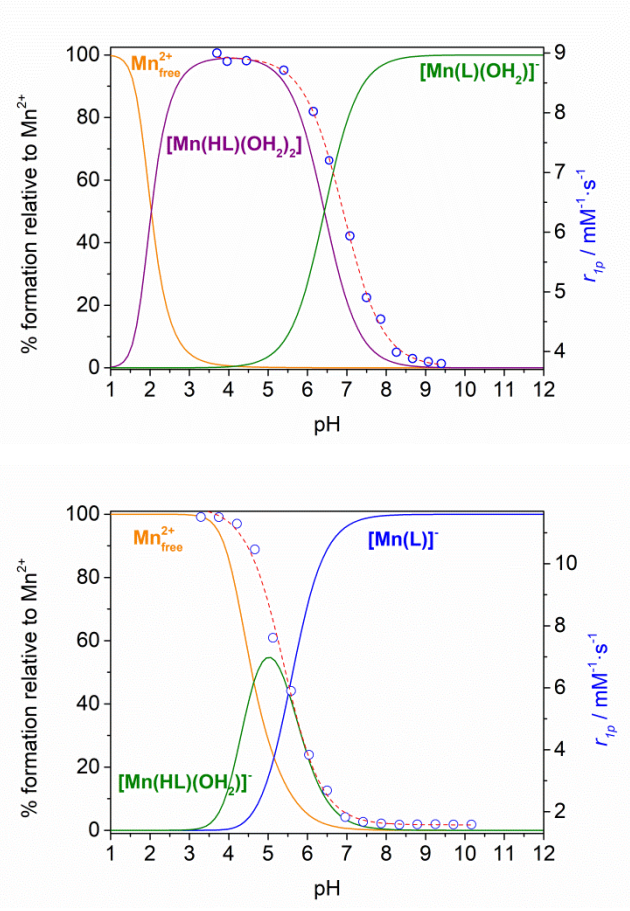

Figure 4. Speciation diagrams calculated for the Mn^{2+}: DPASAm^{3-} (top) and Mn^{2+}: NO2ASAm^{3-} (bottom) systems. $[Mn^{2+}] = [L] = 10^{-3}$ M. Circles represent the relaxivities of [Mn(DPASAm)]$^-$ (top) and [Mn(NO2ASAm)]$^-$ (bottom) recorded at different pH values (298 K, 10 MHz).

The stability constants of the Mn^{2+} complexes were determined using spectrophotometric (DPASAm^{3-}) or potentiometric (NO2ASAm^{3-} and NOTA^{3-}) titrations. The absorption spectra of the Mn^{2+}:DPASAm^{3-} system experience important changes with pH (Figure 3). The intensity of the absorption maximum at 269 nm decreases in the pH range 1.3-3.4 as the protonated complex [Mn(HDPASAm)] is formed. The deprotonation and coordination of the sulfonamide pendant induces a second decrease of the absorbance at 269 nm above pH ~4.5 until pH ~ 7.8.

The stability of the NOTA^{3-} complex was also investigated using potentiometry for comparative purposes. The stability constant of the Mn^{2+} complexes with NOTA^{3-} determined in 0.15 M NaCl (logK_{MnL} = 15.6) is slightly lower than that reported in 0.1 M Me_4NCl (logK_{MnL} = 16.3). These values are in turn slightly higher than those reported initially by Sherry et al. in 0.1 M Me_4NCl (logK_{MnL} = 14.9).[39]

The stability constants determined for the Mn^{2+} complexes of DPASAm^{3-} and NO2ASAm^{3-} are comparable to those of the parent carboxylate analogues DPAAA^{3-} and NOTA^{3-}. However, the high basicity of the sulfonamide group provokes a significant decrease of the conditional stability at physiologically relevant pH values. This is reflected in the calculated pMn values, which define the stability of the complexes under specific conditions.[40] The pMn value determined for the NO2ASAm^{3-} complex is one unit lower than that of DPAAA^{3-}, with an even more pronounced effect observed by comparing the pMn values of the NO2ASAm^{3-} and NOTA^{3-} complexes. The lower basicity of DPAAA^{3-} is also responsible for the high pMn value compared to NOTA^{3-}, in spite of the fact that logK_{MnL} is more than two orders of magnitude higher for the latter.

Both the [Mn(DPASAm)]$^-$ and [Mn(NO2ASAm)]$^-$ complexes protonate at relatively high pH values, with logK_{MnHL} values of 6.43 and 5.52, respectively. These protonation events can be ascribed to the protonation of the sulfonamide group. The decrease of 4-5 orders of magnitude in the protonation constants of the sulfonamides in the presence of Mn^{2+} confirms the coordination of the sulfonamide N atom to the metal ion, as observed in the solid state (see above). The coordinated sulfonamide group is more basic in [Mn(DPASAm)]$^-$ than in [Mn(NO2ASAm)]$^-$. This likely reflects a stronger coordination of the sulfonamide N atom in the six-coordinate [Mn(NO2ASAm)]$^-$ complex compared to the seven-coordinate [Mn(DPASAm)]$^-$ analogue.

The speciation diagrams calculated for the Mn^{2+}: DPASAm^{3-} and Mn^{2+}: NO2ASAm^{3-} systems, using the equilibrium constants given in Table 2, clearly confirm the higher stability of the [Mn(DPASAm)]$^-$ complex, which protonates below

pH ~ 9 and exists largely as the protonated form in the pH range 5-4 (Figure 4). Below pH ~ 4 complex dissociation takes place. Conversely, [Mn(NO2ASAm)]$^-$ protonates at a lower pH (< ~ 8.0), dissociating already below pH 7.0. As a result, the maximum concentration of the protonated species is observed at pH 5.1 (55%), with 18 and 27% of the total manganese being present as the anionic complex and the free metal ion, respectively. The [Mn(NOTA)]$^-$ complex dissociates below pH~5 (Figure S9, Supporting Information).

Relaxometric study. The potential response of [Mn(DPASAm)]$^-$ and [Mn(NO2ASAm)]$^-$ to changes in pH was analyzed by measuring proton relaxivities (r_{1p}) of aqueous solutions of the complexes at 10 MHz and 25 ºC. The [Mn(NO2ASAm)]$^-$ complex presents a low and constant relaxivity of 1.6 mM^{-1}s^{-1} in the pH range 7-10 (Figure 4). This relaxivity is characteristic of Mn^{2+} complexes that lack coordinated water molecules ($q = 0$), the observed relaxivity being the result of the outer-sphere contribution.[41] The outer-sphere contribution is the result of the dipolar coupling between the electron spin of the paramagnetic center and the nuclear spins of water molecules diffusing in the proximity of the paramagnetic complex. Lowering the pH below pH 7 results in a sharp increase of r_{1p}, which reaches a value of 11.5 mM^{-1}s^{-1} at pH 2.5. This is in good agreement with the species distribution diagram reported in Figure 4, which shows that protonation of the complex occurs below pH ~ 8 and complex dissociation below pH ~ 7. Thus, the relaxivity increase observed below pH ~7 is likely related to both complex protonation and dissociation. To confirm this, we recorded ^{1}H Nuclear Magnetic Relaxation Dispersion (NMRD) profiles at pH 4.0. The NMRD profile shows the dispersion in the range 3-20 MHz typical of small Mn^{2+} complexes, together with a second dispersion below 1 MHz that is characteristic of the scalar contribution to relaxivity in the aquated $[Mn(H_2O)_6]^{2+}$ complex (Figure 5, see also Figure S10, Supporting Information).[42,43] This indicates that at pH 4 the complex is largely dissociated, in line with the speciation diagram shown in Figure 4.

The relaxivity of the [Mn(NO2ASAm)]$^-$ complex was further analyzed by recording ^{1}H NMRD profiles at pH 8.0 and three different temperatures (283, 298 and 310 K) in the proton Larmor frequency range 0.01 – 120 MHz (Figure 6). ^{1}H relaxivity decreases with increasing temperature, as expected due to the increase of the relative translational diffusion coefficient D_{MnH}.[44] The relaxivities observed for [Mn(NO2ASAm)]$^-$ were analyzed using Freed's outer-sphere model.[45] The fits of the NMRD data were performed by assuming a value of 3.6 Å for a_{MnH}, the distance of closest approach of proton nuclei of outer sphere water molecules to the paramagnetic ion. All other parameters were determined from the least-squares fit of the data (Table 3).

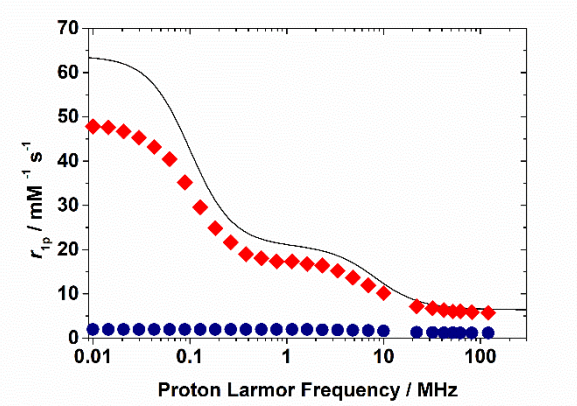

Figure 5. Comparison between the ^{1}H NMRD profile of [Mn(NO2ASAm)]$^-$ recorded at pH 8.0 (blue circles), pH 4.0 (red diamonds) and the ^{1}H NMRD profile of $[Mn(H_2O)_6]^{2+}$ reported in ref **¡Error! Marcador no definido.**. All data were acquired at 298 K.

Table 3. Parameters obtained from the fits of ^{1}H NMRD data.

	[Mn(HDPASAm)]	[Mn(DPASAm)]$^-$	[Mn(NO2ASAm)]$^-$	[Mn(DPAMeA)] [b]	[Mn(DPAAA)]$^-$ [c]
k_{ex}^{298} / 10^7 s^{-1}	30.6[a]	-	-	30.6	12.6
$\Delta H^{\ddagger}$ / kJ mol^{-1}	28.1[a]	-	-	28.1	42.7
τ_R^{298} / ps	72.0 ± 0.8	99.4 ± 4.4	-	47.8	47.6
E_r / kJ mol^{-1}	23.9 ± 0.5	21.6 ± 1.8	-	25.3	22.8
τ_v^{298}/ ps	56 ± 2	14.3 ± 0.06	15.6 ± 0.9	39.2	19.4
D_{MnH}^{298} / 10^{-10} m^2 s^{-1}	22.3[a]	22.3[a]	22.3± 0.2	22.4	22.4
E_{DMnH}/ kJ mol^{-1}	23[a]	23[a]	23 ± 5	17.3	17.3
Δ^2 / 10^{20} s^{-2}	0.130 ± 0.010	0.76 ± 0.05	1.7 ± 0.1	0.238	0.55
r_{MnH} / Å	2.741[a]	2.741[a]	-	2.74	2.756[a]
a_{MnH} / Å	3.6[a]	3.6[a]	3.6[a]	3.6	3.6[a]
q^{298}	2[a]	1[a]	0[a]	2	1[a]

[a] Parameters fixed during the fitting procedure. [b] Data from reference 23. [c] Data from reference 22.

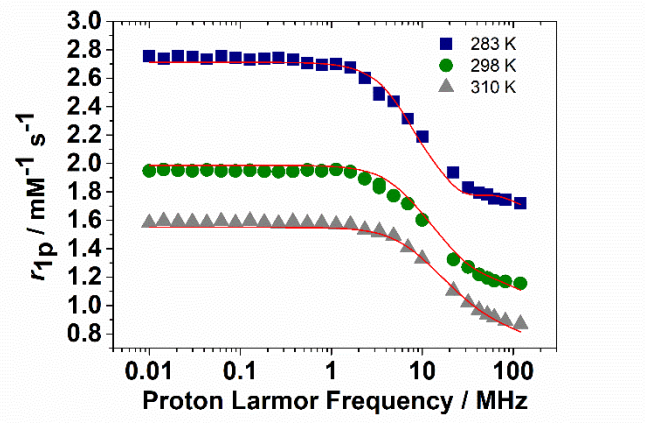

Figure 6. ^{1}H NMRD profiles of [Mn(NO2ASAm)]$^-$ recorded at pH 8.0. The solid lines correspond to the fit of the data as described in the text.

The values of the relative diffusion coefficient D_{MnH}^{298} and its activation energy E_{DMnH} are very similar to those determined for the self-diffusion of water in water (23×10^{-10} m^{2}s^{-1} and 17.6 kJ mol^{-1}, respectively).[46] This is expected, as D_{MnH}^{298} is the sum of the self-diffusion coefficients of water molecules and the paramagnetic species, and water diffuses much faster than the complex. Thus, these parameters support the reliability of the analysis, indicating that the value assumed for a_{MnH} is reasonable.

The relaxivity of the DPASAm^{3-} complex at pH 9 (10 MHz, 25 ºC, 3.8 mM^{-1} s^{-1}) is compatible with the presence of a water molecule in the first coordination sphere of the metal ion. Decreasing the pH of the solution causes an important increase in relaxivity, which reaches a value of 8.9 mM^{-1} s^{-1} in the pH range 5.5-4.0 (Figure 4). This behavior can be attributed to the protonation and decoordination of the sulfonamide group, which allows a second water molecule to enter the Mn^{2+} coordination environment, yielding a bis-hydrated complex at low pH. The analysis of the r_{1p} vs pH dependence yields a pK_a of 6.90 $\pm$ 0.02. This value differs slightly from that obtained with potentiometric measurements (pK_a = 6.43, Table 2), likely as a result of the different ionic strengths used in the two experiments.

The ^{1}H NMRD profiles of the DPASAm^{3-} complex were recorded at three temperatures and pH values of 9.1 and 4.7 (Figure 7), so that the non-protonated [Mn(DPASAm)]$^-$ and the protonated [Mn(HDPASAm)] species are largely dominant (Figure 4). The relaxivities observed at low pH are higher than those determined at basic pH over the whole range of proton Larmor frequencies, in line with an increased hydration number upon complex protonation.

The inner-sphere contribution to relaxivity ($r_{1p,is}$) in Mn^{2+} complexes depends on the relaxation rate of inner sphere protons (T_{1m}^H), the mean residence time of a water molecule in the inner coordination sphere of the metal ion (τ_m=1/k_{ex}) and the number of inner-sphere water molecules q:[47]

$$r_{1p,is} = \frac{1}{1000} \times \frac{q}{55.55} \times \frac{1}{T_{1m}^H + \tau_m} \qquad (1)$$

The relaxation rate of inner sphere protons in Mn^{2+} complexes other than the aqua-ion is generally dominated by the dipole-dipole (DD) mechanism:[48]

$$\left(\frac{1}{T_{1m}^H}\right)^{DD} = \frac{2}{15}\left(\frac{\mu_0}{4\pi}\right)^2 \frac{\gamma_I^2 g^2 \mu_B^2}{r_{MnH}^6} S(S+1)\left(\frac{3\tau_{d1}}{1+\omega_I^2\tau_{d1}^2} + \frac{7\tau_{d2}}{1+4\omega_s^2\tau_{d2}^2}\right) \qquad (2)$$

In Eq (2), g is the electron g factor, r_{MnH} is the distance between the electron and nuclear spins, μ_B is the Bohr magneton, γ_I is the ^{1}H gyromagnetic ratio, S is the total spin (5/2 for a high-spin Mn^{2+} complex), ω_I is the proton resonance frequency and ω_S is the Larmor frequency of the Mn^{2+} electron spin. The correlation time τ_{di} is given by Eq (3), where τ_R is the rotational correlation time, and T_{ie} are the longitudinal (i=1) and transverse (i = 2) relaxation times of the electron spin.

$$\frac{1}{\tau_{di}} = \frac{1}{\tau_R} + \frac{1}{\tau_m} + \frac{1}{T_{ie}}, \text{with } i = 1,2 \quad (3)$$

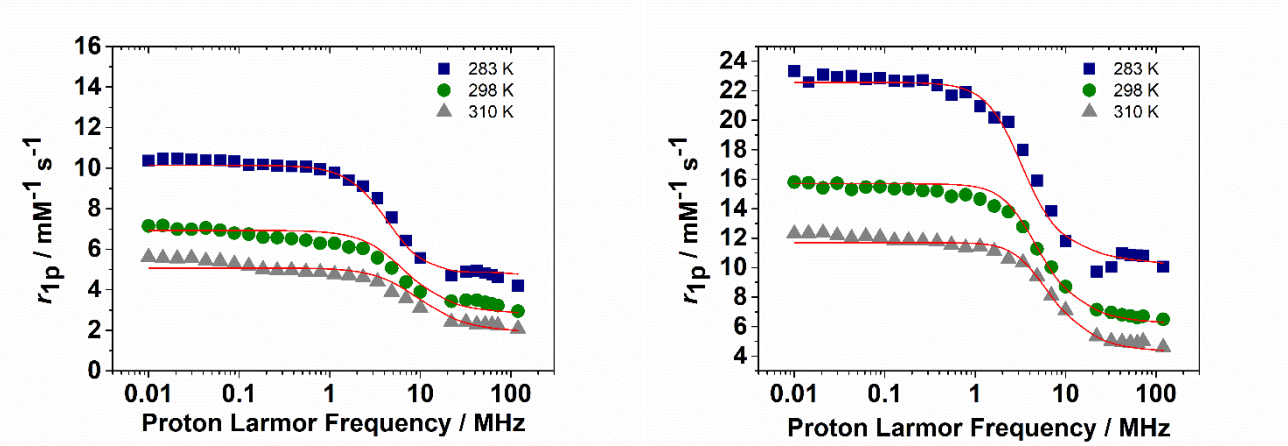

Figure 7. ^{1}H NMRD profiles of the Mn^{2+} complex of DPASAm^{3-} recorded at pH 9.1 (left) and 4.7 (right). The solid lines correspond to the fit of the data as described in the text.

The τ_R values characteristic of small Mn^{2+} complexes are typically < 100 ps, while τ_m is generally in the ns time scale. Furthermore, most often T_{1m}^H is longer than τ_m, so that water exchange has little effect in Eq (1). As a result, ^{1}H NMRD profiles are quite often insensitive to water exchange. Unfortunately, the low solubility of the $DPASAm^{3-}$ complex prevented us from recording ^{17}O NMR measurements, which provide direct access to water exchange dynamics.[49]

The ^{1}H NMRD profiles recorded at basic pH, where the $[Mn(DPASAm)]^-$ species largely dominates the speciation in solution, could be fitted very well by assuming that τ_m provides a negligible contribution to Eqs (1) and (3) (Table 3 and Figure 7). Furthermore, we also fitted the temperature dependence of r_{1p} recorded at 32 MHz in the temperature range 283-323 K (Figure S11, Supporting Information). The fit of the data was carried out by fixing some of the parameters to reasonable values: the diffusion coefficient and its activation energy were fixed to the values obtained for $[Mn(NO2ASAm)]^-$, a_{MnH} was set to 3.6 Å, the number of coordinated water molecules was assumed to be q=1, and r_{MnH} was fixed to the average $Mn\cdots H_{water}$ distance observed in the X-ray structure of the complex described above. The fit of the data provided a τ_R^{298} value (99 ps) that is very reasonable considering the size of the complex.[23] The parameters characterizing the relaxation of the electron spin, the mean square transient ZFS energy (Δ^2) and its correlation time (τ_v), take values that are in the normal range observed for Mn^{2+} complexes.

The ^{1}H NMRD profiles recorded at pH 4.7, where the protonated [Mn(HDPASAm)] complex is the dominant species, together with the temperature dependence of r_{1p} at 32 MHz, were also analyzed quantitatively. Attempts to fit the data using the same approach applied for the data at high pH did not reproduce well the experimental data, particularly at low temperatures. This suggests that the contribution of τ_m to Eq (3) is not negligible. In the absence of ^{17}O NMR data due to solubility limitations, we hypothesized that the [Mn(HDPASAm)] complex must present a water exchange rate very similar to [Mn(DPAMeA)], as the two species are expected to present very similar coordination environments: a pentagonal bipyramidal coordination where the equatorial plane is defined by the amine N atom and the donor atoms of the two picolinate units, with two water molecules occupying the axial positions.[23]

A very good fit of the experimental data was obtained by fixing k_{ex}^{298} and $\Delta H^{\ddagger}$ to the values determined for [Mn(DPAMeA)] from ^{17}O NMR measurements (Table 3).[23] This analysis yielded a τ_R^{298} value (72 ps) that is somewhat shorter than at basic pH, likely because of an increased flexibility of the complex upon decoordination of the sulfonamide pendant.

The value of Δ^2 varies significantly depending on the nature of the axial donor, being lower for the complex at low pH, where two water molecules occupy the axial positions. The ZFS energy is very sensitive to the symmetry of the coordination environment, increasing as the symmetry is lowered.[50] Thus, it is reasonable that the presence of two different donor atoms in axial positions (water and sulfonamide N atom) results in a higher ZFS energy. A similar trend can be observed by comparing the Δ^2 values reported for [Mn(DPAMeA)] and $[Mn(DPAAA)]^-$ (Table 3). In the latter case, a carboxylate oxygen atom occupies one of the axial positions in the pentagonal bipyramidal coordination environment.[22]

CONCLUSIONS

In this work we have presented two ligands containing a sulfonamide pendant and their Mn^{2+} complexes, which were conceived as potential pH-responsive MRI agents. In the case of $[Mn(DPASAm)]^-$, protonation of the sulfonamide group was observed close to the physiologically relevant pH range. Complex protonation provokes a 2.3-fold increase in ^{1}H relaxivity from r_{1p} = 3.8 mM^{-1} s^{-1} at pH 9.0 to r_{1p} = 8.9 mM^{-1} s^{-1} at pH 4.0 (20 MHz, 25 ºC). Relaxometric and potentiometric studies are in good mutual agreement, showing that the complex is perfectly stable in the pH range 4-10. The X-ray structure of the $[Mn(DPASAm)]^-$ complex evidences coordination of the deprotonated sulphonamide N atom, as well as the presence of a coordinated water molecule. The relaxometric characterization showed that the relaxivity increase observed upon complex protonation is related to the coordination of a second water molecule.

The $[Mn(NO2ASAm)]^-$ complex is also protonated, though the sulfonamide group was found to be considerably less basic than in $[Mn(DPASAm)]^-$ (pK_a = 5.5 and 6.4, respectively). This can be attributed to a stronger $Mn\text{-}N_{sulfonamide}$ interaction in $[Mn(NO2ASAm)]^-$ due to the lower coordination number of the metal ion. Besides the lower pK_a, $[Mn(NO2ASAm)]^-$ is characterized by a lower conditional stability than $[Mn(DPASAm)]^-$, associated to a high basicity of the macrocyclic structure. As a result, the $[Mn(NO2ASAm)]^-$ complex dissociates at a relatively high pH. These results highlight that ligand basicity plays a key role in the stability of potential Mn^{2+} MRI contrast agents, so that this issue should be carefully considered for ligand design. Overall, the results reported in this paper provide a prove of concept on the design of pH-responsive Mn^{2+} MRI probes based on reversible binding of sulfonamide groups, though further probe optimization to improve kinetic inertness is required for practical applications, as the $[Mn(DPASAm)]^-$ complex dissociates very quickly when challenged with an excel of Cu^{2+} (Figure S35, Supporting Information). Another aspect that must be considered is the biodistribution of the probe, as the intensity of the MRI signal will depend both on the protonation state of the complex and the local concentration of the agent.

EXPERIMENTAL SECTION

Materials and methods. Ethyl 6-(chloromethyl)picolinate[51] was prepared following the literature methods. Di-*tert*-butyl 2,2'-(1,4,7-triazonane-1,4-diyl)diacetate (NO2AtBu) was purchased from CheMatech (Dijon, France). All other reagents were purchased from Aldrich Chemical Co.

High resolution electrospray-ionization time-of-flight ESI-TOF mass spectra were recorded using a LC-Q-q-TOF Applied Biosystems QSTAR Elite spectrometer in positive and negative mode. Mass spectra recorded using electron impact ionization were recorded with a Thermo MAT95XP instrument. Elemental analyses were accomplished on a ThermoQuest Flash EA 1112 elemental analyzer. Medium performance liquid chromatography (MPLC) was carried out using a Puriflash XS 420 instrument equipped with a reverse-phase Puriflash 15C18HP column (60 Å, spherical 15 µm, 20 g) and UV-DAD detection at 210 and 254 nm, and operating at a flow rate of 10 mL/min. Aqueous solutions were lyophilized using a Telstar Cryodos-80 apparatus. ^{1}H, ^{13}C and ^{19}F NMR spectra of the ligands and their precursors were recorded at 298 K in using a Bruker AVANCE III 300 or Bruker Avance 500 spectrometers. ^{19}F chemical shifts were referenced by using sodium triflate on a D_2O solvent (δ 75.6 ppm).

***N*-(2-aminoethyl)-4-(trifluoromethyl)benzenesulfonamide (1).** This compound was prepared using a slight modification of the synthesis reported in the literature.[52] A solution of 4-(trifluoromethyl)benzenesulfonyl chloride (0.500 g, 2.044 mmol) in CH_2Cl_2 (20 mL) was added to a solution of ethylendiamine (1.228 g, 20.43 mmol) in CH_2Cl_2 (200 mL) at 0 ºC. The mixture was stirred at room temperature for 16 h and then extracted with 1M HCl (3 x 100 mL). The combined aqueous phases were basified to pH 10 with NaOH and extracted with CH_2Cl_2 (3 x 100 mL). The organic extracts were dried with Na_2SO_4 and concentrated, affording **1** as a white solid (0.502 g, 1.871 mmol, 92% yield). ^{1}H NMR (300 MHz, $CDCl_3$) δ 8.01 (d, J = 8.2 Hz, 2H), 7.79 (d, J = 8.2 Hz, 2H), 3.00 (t, J = 5.6 Hz, 2H), 2.93 – 2.71 (m, 2H). ^{19}F NMR (282 MHz, $CDCl_3$) δ -63.1. MS(ESI$^+$): *m*/*z* calcd for $C_9H_{12}F_3N_2O_2S$ [M + H]$^+$: 269.06. Found: 269.06.

Diethyl 6,6'-(((2-((4-(trifluoromethyl)phenyl)sulfonamido)ethyl)azanediyl)bis-(methylene))dipicolinate (2). A solution of ethyl 6-(chloromethyl)picolinate (0.2981 g, 1.493 mmol) in dry CH_3CN (3 mL) was added dropwise to a solution of compound **1** (0.2001g, 0.75 mmol) containing K_2CO_3 (0.2577g, 1.864 mmol) in dry CH_3CN (35 mL). A catalytic amount of KI was added and the mixture was purged with an argon flow while stirred at room temperature for 6 days. The reaction mixture was filtered and the filtrate was evaporated to dryness in vacuo. The product was purified by MPLC on neutral alumina (CH_2Cl_2:MeOH 90:10 (v:v)) and isolated as a yellow oil (0.2752 g, 62% yield). ^{1}H NMR (300 MHz, $CDCl_3$) δ 8.04 (m, 2H), 7.97 (m, 2H), 7.45 – 7.80 (m, 6H), 7.11 (b, 1H), 4.51 (q, ^3J = 7.1 Hz, 4H), 3.89 (s, 4H), 3.14 (b, 2H), 2.84 (m, 2H), 1.46 (t, ^3J = 7.1 Hz, 6H). ^{19}F NMR (282 MHz, $CDCl_3$) δ -63.0. ^{13}C NMR (75.5 MHz, $CDCl_3$) δ 165.0, 159.4, 147.6, 144.4, 137.4, 133.5 ($^1J_{C\text{-}F}$ = 32.2 Hz), 127.5, 126.3, 125.9, 123.5, 61.8, 59.5, 53.8, 41.3, 14.2. MS(ESI$^+$): *m*/*z* calcd for $C_{27}H_{29}F_3N_4NaO_6S$ [M + Na]$^+$: 617.17. Found: 617.17.

H_3DPASAm. Compound **2** (0.2501 g, 0.4206 mmol) was dissolved in 6M HCl (20 mL) and the mixture was heated at 55 ºC for 16 h. The acid was evaporated, water (3 mL) was added and evaporated again twice to remove most of the HCl. The ligand was isolated by filtration as a white solid (0.1435 g, 0.2528 mmol, 60% yield). ^{1}H NMR (500 MHz, D_2O, pH 14) δ 7.50-7.65 (m, 8H), 7.18 (m, 2H), 3.60 (s, 4H), 2.63 (m, 2H), 2.33 (m, 2H). ^{19}F NMR (376 MHz, D_2O, pH 14) δ -62.5. ^{13}C NMR (126 MHz, D_2O, pH 14) δ 172.7, 168.4, 157.6, 152.5, 146.5, 138.1, 126.5, 125.7, 125.3, 122.2, 60.0, 55.6, 42.2. HRMS(ESI$^-$): *m*/*z* calcd for $C_{23}H_{20}F_3N_4O_6S$ [M - H]$^-$: 537.1061. Found: 537.1064. Elemental analysis: calculated for $C_{23}H_{21}F_3N_4O_6S{\cdot}0.8HCl$: C: 48.84; H: 3.69; N: 9.54. Found: C: 48.66; H: 3.87; N: 9.87. IR (ATR, ϋ[cm^{-1}]): 1738 ν(C=O), 1575 ν(C=N), 1356, 1322, 1164 ν(S=O).

***N*-(2-bromoethyl)-4-(trifluoromethyl)benzene sulfonamide (3).** The synthesis followed the procedure reported for closely related compounds.[53] 2-Bromoethan-1-amine hydrobromide (0.4702 g, 2.295 mmol, 1 eq) and triethylamine (0.640 mL, 4.59 mmol, 2 eq) were dissolved in CH_2Cl_2 (15 mL). 4-(Trifluoromethyl)benzene sulfonyl chloride (0.5614 g, 2.295 mmol, 1 eq) dissolved in CH_2Cl_2 (2 mL) was added dropwise to the solution while stirring at room temperature. The yellowish solution was stirred for 24h. The solution was washed with 1M HCl (3 x 15 mL) followed by brine (10 mL). The organic layer was dried using Na_2SO_4, filtered and the solvent was evaporated. The white solid was washed with acidified water (pH 5; 2 x 10 mL) and dried (0.6154 g, 1.853 mmol, 81% yield). ^{1}H NMR (300 MHz, $CDCl_3$): δ 8.02 (d, ^3J = 8.5 Hz, 2H), 7.81 (d, ^3J = 8.5 Hz, 2H), 5.24 (b, 1H), 3.43 (m, 4H). ^{19}F NMR (282 MHz, $CDCl_3$): -63.1. ^{13}C NMR (75.5 MHz, $CDCl_3$): δ 143.5, 127.5, 126.5 ($^2J_{C\text{-}F}$ = 3.8 Hz), 44.6, 31.5. MS(EI, 70 eV): *m*/*z* calcd for $C_9H_9BrF_3NO_2S$ [M$^+$]: 330.9. Found: 330.9. Elemental analysis: calculated for $C_9H_9BrF_3NO_2S$: C: 32.55; H: 2.73; N: 4.22; S: 9.65. Found: C: 33.07; H: 2.62; N: 3.93; S: 9.54.

2,2'-(7-(2-((4-(Trifluoromethyl)phenyl) sulfonamido)ethyl)-1,4,7- triazonane-1,4-diyl)diacetate (4). Di-*tert*-Butyl 2,2'-(1,4,7-triazacyclononane-1,4-diyl)diacetate (0.1999 g, 0.5592 mmol, 1 eq) was dissolved in dry CH_3CN (10 mL) and K_2CO_3 (0.1932 g, 1.398 mmol) was added under argon. The mixture was stirred at room temperature and compound **3** (0.1857 g, 0.5591 mmol, 1 eq) dissolved in CH_3CN (5 mL) was added. The mixture was heated and stirred at 60 ºC 24 h and then the carbonate was removed by filtration. The evaporation of the solvent yielded a yellowish oil that was purified on neutral alumina using MPLC (CH_2Cl_2/MeOH (10%)). The fractions containing the product were concentrated affording a yellow oil (0.3297 g, 0.5416 mmol, 97% yield). ^{1}H NMR (300 MHz, $CDCl_3$) δ 8.00 (d, ^3J = 8.3 Hz, 2H), 7.75 (d, ^3J = 8.3 Hz, 2H), 3.31 (s, 4H), 3.02 (t, ^3J = 5.4 Hz, 2H), 2.87 – 2.59 (m, 14H), 1.44 (s, 18H). ^{19}F NMR (282 MHz, $CDCl_3$): δ -63.0. ^{13}C NMR (126 MHz, $CDCl_3$): 171.3, 144.4, 133.8 (^1J = 32.9 Hz), 127.5, 126.0 (^2J = 3.6 Hz), 80.9, 58.9, 56.0, 55.3, 55.0, 54.7, 28.2. HRMS(ESI$^+$): *m*/*z* calcd for $C_{27}H_{44}F_3N_4O_6S$ [M + H]$^+$: 609.2928. Found: 609.2916. IR (ATR, ϋ[cm^{-1}]): 1733 ν(C=O), 1323, 1159, 1129 ν(S=O).

H_3NO2ASAm. Compound **4** (0.1240 g, 0.2037 mmol) was dissolved in 3M HCl (20 mL) and the mixture was stirred 24 h at room temperature. The acid was evaporated, water (3 mL) was added and evaporated again twice to remove most of the HCl. The product was lyophilized to afford a white solid (0.1096 g, 0.1838 mmol, 90% yield). ^{1}H NMR (500 MHz, D_2O, pH 1.5): 8.07 (d, ^3J = 8.3 Hz, 2H), 7.99 (d, ^3J = 8.3 Hz, 2H), 3.83 (s, 4H), 3.53 – 3.30 (m, 12H), 3.18 (s, 4H). ^{19}F NMR (282 MHz, D_2O, pH 1.5): δ -63.1. ^{13}C NMR (126 MHz, D_2O, pH 1.5): 173.9, 140.8, 134.5 ($^1J_{C\text{-}F}$ = 32.7 Hz), 127.6, 126.9 ($^2J_{C\text{-}F}$ = 3.7 Hz), 56.4, 55.4, 51.1, 49.9, 48.5, 38.3. HRMS(ESI$^+$): *m*/*z* calcd for $C_{19}H_{28}F_3N_4O_6S$ [M + H]$^+$: 497.1676. Found: 497.1668. Elemental analysis: calculated for $C_{19}H_{27}F_3N_4O_6S{\cdot}2HCl{\cdot}1.5H_2O$: C: 38.26; H: 5.41; N: 9.39; S: 5.38. Found: C: 38.38; H: 5.14; N: 9.03; S: 5.03. IR (ATR, ϋ[cm^{-1}]): 1732 ν(C=O), 1321, 1163 ν(S=O).

Potentiometric and spectrophotometric measurements. Ligand protonation constants and stability and protonation constants of the Mn^{2+} complexes were determined by potentiometric or spectrophotometric titrations, using the HYPERQUAD2013 program.[54] All measurements were carried out at 298 K with an ionic strength adjusted to 0.15 M using NaCl. Stability constants of the metal complexes were obtained from titrations at 1:1 metal to ligand concentration ratio. The $MnCl_2$ solution was standardized by titration with EDTA at pH 10 (NH_3/NH_4Cl buffer) in the presence of triethanolamine to avoid manganese precipitation. Eriochrome black T was employed as indicator.[55] The concentration of the solution was double checked by titrating chloride with $AgNO_3$ using potassium chromate as indicator.[55]

Potentiometric titrations were carried out with a dual-wall cell thermostated at 298 K using circulating water. All measurements were performed with magnetic stirring to homogenize

the solutions (starting volume 10 mL), while bubbling nitrogen on the surface of the solution to avoid CO_2 absorption. The concentration of the ligand in the titration cell was 2-3 mM, while titrations covered the pH range of ca. 2.0 to 12.0. The solution of the ligand, in the absence and presence of the metal ion, was titrated with standard solutions of hydrochloric acid or sodium hydroxide. The titrant was delivered with a Crison microBu 2030 automatic burette using 2.5 mL or 1.0 mL syringes. A Crison micropH 2000 pH-meter, connected to a glass electrode (Radiometer pHG211) and a reference electrode (Radiometer REF201), was used to measure the electromotive force (emf) values. The procedures used for electrode calibration were described in detail elsewhere.[56] The formation of the Mn^{2+} complexes of $DPASAm^{3-}$ and $NO2ASAm^{3-}$ was fast. In the case of the $NOTA^{3-}$ complex the equilibrium was attained more slowly, taking 5-10 min depending on the pH. Back titrations were performed to confirm that the equilibrium was attained.

The UV-vis absorption spectra were recorded with a Uvikon-XS (Bio-Tek Instruments) double-beam spectrophotometer, using cells of 1 cm path length. The spectra were recorded in the range 230-310 nm (80 wave lengths) for every solution. The pH of the solutions below 2.8 or above 11.9 was adjusted directly with standard solutions of hydrochloric acid or sodium hydroxide. Otherwise, different buffers were used to facilitate pH adjustment: borax 0.0125 M (pH range 8 – 10.8), phosphate (pH ranges 5.8-8.0, 0.05 M; and 10.9-12.0, 0.025 M) or acetate (pH range 3.5-5.3, 0.02 M).[57] The HypSpec2014 program was used to determine the equilibrium constants and the spectra of the absorbing species.[54]

Relaxometric measurements. $1/T_1$ ^{1}H Nuclear Magnetic Relaxation Dispersion (NMRD) profiles were measured with a Fast-Field Cycling (FFC) Stelar SmarTracer Relaxometer over a continuum of magnetic field strengths from 0.01 to 10 MHz proton Larmor Frequencies, with an uncertainty in $1/T_1$ of ca. 1%. Data in the 20-120 MHz range were collected with a High Field Relaxometer (Stelar) equipped with the HTS-110 3T Metrology Cryogen-free Superconducting Magnet. The analyses were carried out by using the standard inversion recovery sequence with a typical 90° pulse width of 3.5 μs and the reproducibility of the data was within ± 0.5%. The temperature was controlled with a Stelar VTC-91 heater airflow equipped with a copper-constantan thermocouple (uncertainty of ± 0.1 K).

The Mn^{2+} complexes were prepared by mixing solutions of $MnCl_2$ and the corresponding ligand, using a ~5% molar excess of the latter. The pH was adjusted to ~7.0 with HCl or NaOH. The concentration of Mn^{2+} chelates was assessed by ^{1}H-NMR measurements (Bruker Advance III Spectrometer equipped with a wide bore 11.7 Tesla magnet), by using the well-established Evans's method.[58]

X-ray diffraction measurements. A single crystal of $Na[Mn(DPASAm)(H_2O)]\cdot 2H_2O$ ·was analyzed by X-ray diffraction. Crystallographic data were collected at room temperature using a Bruker Smart 6000 CCD detector and Cu-Kα radiation (λ= 1.54178 Å) generated by an Incoatec microfocus source equipped with Incoatec Quazar MX optics. The software APEX2[59] was used for collecting frames of data, indexing reflections, and the determination of lattice parameters, SAINT[60] for integration of the intensity of reflections, and SADABS[61] for scaling and empirical absorption correction. The structure was solved by dual-space methods using the program SHELXT.[62] All non-hydrogen atoms were refined with anisotropic thermal parameters by full-matrix least-squares calculations on F^2 with the SHELXL-2018/3 program.[63] Hydrogen atoms were inserted at calculated positions and constrained with isotropic thermal parameters except for the hydrogen atom of the water molecules, which were located from a Fourier-difference map and refined isotropically. Crystal data and structure refinement details: Formula: $C_{23}H_{26}F_3MnN_4NaO_{10}S$; MW: 685.47; crystal system: triclinic; space group: P–1; a = 8.9108(6) Å; b = 9.2961(7) Å; c = 17.0716(12) Å; α= 97.133(2)°, β= 95.201(3)°, γ = 97.178(2)°; V= 1384.08(17) Å^3; F(000) = 702; Z = 2; D_{calc}= 1.645 g cm^{-3}; μ = 5.494 mm^{-1}; θ range=4.84– 71.28º; R_{int} = 0.0485; 22598 measured reflections, of which 5243 were independent and 5047 were unique with $I > 2\sigma(I)$. GOF on F^2 = 1.045; $R1$ = 0.0401; $wR2$ (all data) = 0.1036; Largest differences peak and hole: 0.504 and –0.509 eÅ^{-3}.

ASSOCIATED CONTENT

Supporting Information

The supporting Information is available free of charge at http://pubs.acs.org/doi/xxx/xxxx.

Potentiometric titration curves, speciation diagrams, spectrophotometric titrations, relaxometric data, NMR and MS of ligands and their precursors (PDF)

Accession Codes

CCDC 2015848 contains the supplementary crystallographic data for this paper. These data can be obtained free of charge via www.ccdc.cam.ac.uk/data_request/cif, or by emailing data_request@ccdc.cam.ac.uk, or by contacting The Cambridge Crystallographic Data Centre, 12 Union Road, Cambridge CB2 1EZ, UK; fax: + 44 1223 336033.

AUTHOR INFORMATION

Corresponding Authors

Carlos Platas-Iglesias — Centro de Investigacións Científicas Avanzadas (CICA) and Departamento de Química, Universidade da Coruña, 15008 A Coruña, Spain; Email: carlos.platas.iglesias@udc.es.

Mauro Botta — *Dipartimento di Scienze e Innovazione Tecnologica, Università del Piemonte Orientale "A. Avogadro", Viale T. Michel 11, 15121 Alessandria, Italy.* Email: mauro.botta@uniupo.it

Author Contributions

The manuscript was written through contributions of all authors. All authors have given approval to the final version of the manuscript.

Notes

The authors declare no competing financial interest.

ACKNOWLEDGMENT

Authors C. P.-I. and D. E.-G. thank Ministerio de Economía y Competitividad (CTQ2016-76756-P) and Xunta de Galicia (ED431B 2017/59 and ED431D 2017/01) for generous financial support. R.U.-V. thanks Xunta de Galicia (ED481A-2018/314) for funding her PhD contract. M.B., F.C. and D.L. are grateful to Università del Piemonte Orientale per financial support (FARC 2019). M. M.-C. thanks Ministerio de Ciencia e Innovación and Ministerio de Universidades for the Distinguished Research Contract "Beatriz Galindo" (BEAGAL18/00144).

REFERENCES

(1) Wahsner, J.; Gale, E. M.; Rodríguez-Rodríguez, A.; Caravan, P. Chemistry of MRI Contrast Agents: Current Challenges and New Frontiers. *Chem. Rev.* **2019**, *119*, 957–1057.

(2) The Chemistry of Contrast Agents in Medical Magnetic Resonance Imaging, Second Edition, 2nd Edn.; Merbach, A., Helm, L., Tóth, É., Eds.; WILEY, 2013.

(3) Lauterbur, P. C.; Mendoça-Dias, M. H.; Rudin, A. A. Augmentation of Tissue Water Proton Spin-Lattice Relaxation Rates by In Vivo Addition of Paramagnetic Ions, in Frontiers of Biological Energetics, Dutton, P. O.; Leigh, J., Scarpa, A. Eds.; Academic Press, New York, NY, 1978, pp. 752–759.

(4) Brady, T. J.; Gebhardt, M. C.; Pykett, I. L.; Buonanno, F. S.; Newhouse, J. H.; Burt, C. T.; Smith, R. J.; Mankin, H. J.; Kistler, J. P.; Goldman, M. R.; Hinshaw, W. S.; Pohost. G. M. NMR Imaging of Forearms in Healthy Volunteers and Patients with Giant-Cell Tumor of Bone. *Radiology* **1982**, *144*, 549–552.

(5) Goldman, M. R.; Brady, T. J.; Pykett, I. L.; Burt, C. T.; Buonanno, F. S.; Kistler, J. P.; Newhouse, J. H.; Hinshaw, W. S.; Pohost, G. M. Quantification of Experimental Myocardial Infarction Using Nuclear Magnetic Resonance Imaging and Paramagnetic Ion Contrast Enhancement in Excised Canine Hearts. *Circulation* **1982**, *66*, 1012–1016.

(6) Young, I. R.; Clarke, G. J.; Baffles, D. R.; Pennock, J. M.; Doyle, F. H.; Bydder, G. M. Enhancement of Relaxation Rate with Paramagnetic Contrast Agents in NMR Imaging. *Clin. Imag.* **1981**, *5*, 543–547.

(7) Carr, D. H.; Brown, J.; Bydder, G. M.; Weinmann, H. J.; Speck, U.; Thomas, D. J.; Young, I. R. Intravenous Chelated Gadolinium as a Contrast Agent in NMR Imaging of Cerebral Tumours. *Lancet* **1984**, *1*, 484–486.

(8) Sarka, L.; Burai, L.; Brücher, E. The Rates of the Exchange Reactions between $[Gd(DTPA)]^{2-}$ and the Endogenous Ions Cu^{2+} and Zn^{2+}: A Kinetic Model for the Prediction of the In Vivo Stability of $[Gd(DTPA)]^{2-}$, Used as a Contrast Agent in Magnetic Resonance Imaging. *Chem. Eur. J.* **2000**, *6*, 719–724.

(9) Sherry, A. D.; Wu, Y. The Importance of Water Exchange Rates in the Design of Responsive Agents for MRI. *Curr. Opin. Chem. Biol.* **2013**, *17*, 167–174.

(10) Grobner, T. Gadolinium - A Specific Trigger for the Development of Nephrogenic Fibrosing Dermopathy and Nephrogenic Systemic Fibrosis? *Nephrol. Dial. Transplant.* **2006**, *21*, 1104–1108.

(11) Marckmann, P.; Skov, L.; Rossen, K.; Dupont, A.; Damholt, M. B.; Heaf, J. G.; Thomsen, H. S. Nephrogenic Systemic Fibrosis: Suspected Causative Role of Gadodiamide Used for Contrast-Enhanced Magnetic Resonance Imaging. *J. Am. Soc. Nephrol.* **2006**, *17*, 2359–2362.

(12) (a) Kanal, E.; Tweedle, M. F. Residual or Retained Gadolinium: Practical Implications for Radiologists and Our Patients. *Radiology* **2015**, *275*, 630–634; (b) Fraum, T. J.; Ludwig, D. R.; Bashir, M. R.; Fowler, K. J. Gadolinium-Based Contrast Agents: A Comprehensive Risk Assessment. *J. Magn. Reson. Imaging* **2017**, *46*, 338–353.

(13) Le Fur, M.; Caravan, P. The Biological Fate of Gadolinium-Based MRI Contrast Agents: A Call to Action for Bioinorganic Chemists. *Metallomics* **2019**, *11*, 240–254.

(14) Viswanathan, S.; Kovacs, Z.; Green, K. N.; Ratnakar, S. J.; Sherry, A. D. Alternatives to Gadolinium-Based Metal Chelates for Magnetic Resonance Imaging. *Chem. Rev.* **2010**, *110*, 2960–3018.

(15) (a) Gupta, A.; Caravan, P.; Price, W. S.; Platas-Iglesias, C.; Gale, E. M. Applications for Transition-Metal Chemistry in Contrast-Enhanced Magnetic Resonance Imaging. *Inorg. Chem.* **2020**, *59*, 6648−6678; (b) Drahos, B.; Lukes, I.; Toth, E. Manganese(II) Complexes as Potential Contrast Agents for MRI. *Eur. J. Inorg. Chem.* **2012**, 1975–1986; (c) Pan, D.; Schmieder, A. H.; Wickline, S. A.; Lanza, G. M. Manganese-Based MRI Contrast Agents: Past, Present, and Future. *Tetrahedron* **2011**, *67*, 8431–8444.

(16) (a) Gale, E. M.; Atanasova, I. P.; Blasi, F.; Ay, I.; Caravan, P. A Manganese Alternative to Gadolinium for MRI Contrast. *J. Am. Chem. Soc.* **2015**, *137*, 15548–15557; (b) Rolla, G. A.; Platas-Iglesias, C.; Botta, M.; Tei, L.; Helm, L. ^{1}H and ^{17}O NMR Relaxometric and Computational Study on Macrocyclic Mn(II) Complexes. *Inorg. Chem.* **2013**, *52*, 3268–3279; (c) Su, H.; Wu, C.; Zhu, J.; Miao, T.; Wang, D.; Xia, C.; Zhao, X.; Gong, Q.; Song, B.; Ai, H. Rigid Mn(II) Chelate as Efficient MRI Contrast Agent for Vascular Imaging. *Dalton Trans.* **2012**, *41*, 14480–14483; (d) Phukan, B.; Mukherjee, C.; Goswami, U.; Sarmah, A.; Mukherjee, S.; Sahoo, S. K.; Moi, S. C. A New Bis(aquated) High Relaxivity Mn(II) Complex as an Alternative to Gd(III)-Based MRI Contrast Agent. *Inorg. Chem.* **2018**, *57*, 2631−2638; (e) Ndiaye, D.; Sy, M.; Pallier, A.; Même, S.; de Silva, I.; Lacerda, S.; Nonat, A. M.; Charbonnière, L. J.; Tóth, É. Unprecedented Kinetic Inertness for a Mn^{2+}-Bispidine Chelate: A Novel Structural Entry for Mn^{2+}-Based Imaging Agents. *Angew. Chem. Int. Ed.* **2020**, *59*, 11958–11963.

(17) (a) Rodríguez, E.; Roig, A.; Molins, E.; Arús, C.; Quintero, M. R.; Cabañas, M. E.; Cerdán, S.; Lopez-Larrubia, P.; Sanfeliu, C. In vitro Characterization of an Fe_8 Cluster as Potential MRI Contrast Agent. *NMR Biomed.* **2005**, *18*, 300–307; (b) Wang, H.; Jordan, V. C.; Ramsay, I. A.; Sojoodi, M.; Fuchs, B. C.; Tanabe, K. K.; Caravan, P.; Gale, E. M. Molecular Magnetic Resonance Imaging Using a Redox-Active Iron Complex. *J. Am. Chem. Soc.* **2019**, *141*, 5916–5925.

(18) Lux, J.; Sherry, A. D. Advances in Gadolinium-Based MRI Contrast Agent Designs for Monitoring Biological Processes in vivo. *Curr. Opin. Chem. Biol.* **2018**, *45*, 121–130.

(19) Angelovski, G. What We Can Really Do with Bioresponsive MRI Contrast Agents. *Angew. Chem. Int. Ed.* **2016**, *55*, 7038 – 7046.

(20) Heffern, M. C.; Matosziuk, L. M.; Meade, T. J. Lanthanide Probes for Bioresponsive Imaging. *Chem. Rev.* **2014**, *114*, 4496–4539.

(21) Botár, R.; Molnár, E.; Trecsényi, G.; Kiss, J.; Kálmán, F. K.; Tircsó, G. Stable and Inert Mn(II)-Based and pH-Responsive Contrast Agents. *J. Am. Chem. Soc.* **2020**, *142*, 1662–1666.

(22) Forgacs, A.; Pujales-Paradela, R.; Regueiro-Figueroa, M.; Valencia, L.; Esteban-Gomez, D.; Botta, M.; Platas-Iglesias, C. Developing the Family of Picolinate Ligands for Mn^{2+} Complexation. *Dalton Trans.* **2017**, *46*, 1546–1558.

(23) (a) Regueiro-Figueroa, M.; Rolla, G. A.; Esteban-Gómez, D.; de Blas, A.; Rodriguez-Blas, T.; Botta, M.; Platas-Iglesias, C. High Relaxivity Mn^{2+}-Based MRI Contrast Agents. *Chem. Eur. J.* **2014**, *20*, 17300–17305; (b) Forgacs, A.; Regueiro-Figueroa, M.; Barriada, J. L.; Esteban-Gomez, D.; de Blas, A.; Rodriguez-Blas, T.; Botta, M.; Platas-Iglesias, C. Mono-, Bi-, and Trinuclear Bis-Hydrated Mn^{2+} Complexes as Potential MRI Contrast Agents. *Inorg. Chem.* **2015**, *54*, 9576–9587.

(24) Molnar, E.; Camus, N.; Patinec, V.; Rolla, G. A.; Botta, M.; Tircso, G.; Kalman, F. K.; Fodor, T.; Tripier, R.; Platas-Iglesias, C. Picolinate-Containing Macrocyclic Mn^{2+} Complexes as Potential MRI Contrast Agents. *Inorg. Chem.* **2014**, *53*, 5136–5149.

(25) (a) Pujales-Paradela, R.; Carniato, F.; Esteban-Gomez, D.; Botta, M.; Platas-Iglesias, C. Controlling water exchange rates in potential Mn^{2+}-based MRI agents derived from $NO2A^{2-}$. *Dalton Trans.* **2019**, *48*, 3962–3972; (b) Patinec, V.; Rolla, G. A.; Botta, M.; Tripier, R.; Esteban-Gomez, D.; Platas-Iglesias, C. Hyperfine Coupling Constants on Inner-Sphere Water Molecules of a Triazacyclononane-based Mn(II) Complex and Related Systems Relevant as MRI Contrast Agents. *Inorg. Chem.* **2013**, *52*, 11173–11184.

(26) Forgács, A.; Tei, L.; Baranyai, Z.; Esteban-Gómez, D.; Platas-Iglesias, C.; Botta, M. Optimising the relaxivities of Mn^{2+} complexes by targeting human serum albumin (HSA). *Dalton Trans.* **2017**, *46*, 8494–8504.

(27) (a) Lowe, M. P.; Parker, D.; Reany, O.; Aime, S.; Botta, M.; Castellano, G.; Gianolio, E.; Pagliarin, R. pH-Dependent Modulation of Relaxivity and Luminescence in Macrocyclic Gadolinium

and Europium Complexes Based on Reversible Intramolecular Sulfonamide Ligation. *J. Am. Chem. Soc.* **2001**, *123*, 7601–7609; (b) Lowe, M. P.; Parker, D. Controllable pH Modulation of Lanthanide Luminescence by Intramolecular Switching of the Hydration State. *Chem. Commun.* **2000**, 707–708; (c) Takács, A.; Napolitano, R.; Purgel, M.; Bényei, A. C.; Zékány, L.; Brücher, E.; Tóth, I.; Baranyai, Z.; Aime, S. Solution Structures, Stabilities, Kinetics, and Dynamics of DO3A and DO3A−Sulphonamide Complexes. *Inorg. Chem.* **2014**, *53*, 2858−2872; (d) Moriggi, L.; Yaseen, M. A.; Helm, L.; Caravan, P. Serum Albumin Targeted, pH-Dependent Magnetic Resonance Relaxation Agents. *Chem. Eur. J.* **2012**, *18*, 3675–3686.

(28) (a) Casanova, D.; Alemany, P.; Bofill, J. M.; Alvarez, S. Shape and Symmetry of Heptacoordinate Transition-Metal Complexes: Structural Trends. *Chem. Eur. J.* **2003**, *9*, 1281–1295; (b) Regueiro-Figueroa, M; Lima, L. M. P.; Blanco, V.; Esteban-Gómez, D.; de Blas, A.; Rodríguez-Blas, T.; Delgado, R.; Platas-Iglesias, C. Reasons Behind the Relative Abundances of Heptacoordinate Complexes along the Late First-Row Transition Metal Series, *Inorg. Chem.* **2014**, *53*, 12859−12869.

(29) (a) Huang, Q.; Zhai, B. Crystal Structure, Thermal and Magnetic Studies of a Dinuclear Mn(II) Complex with Decadentate Picolinate Based Ligand. *J. Coord. Chem.* **2007**, *60*, 2257−2263; (b) Khannam, M.; Weyhermüller, T.; Goswami, U.; Mukherjee, C. A Highly Stable L-Alanine-Based Mono(aquated) Mn(II) Complex as a T_1-Weighted MRI Contrast Agent. *Dalton Trans.* **2017**, *46*, 10426−10432; (c) Gerey, B.; Gennari, M.; Gouré, E.; Pécaut, J.; Blackman, A.; Pantazis, D.; Neese, F.; Molton, F.; Fortage, J.; Duboc, C.; Collomb, M.-N. Calcium and Heterometallic Manganese–Calcium Complexes Supported by Tripodal Pyridinecarboxylate Ligands: Structural, EPR and Theoretical Investigations. *Dalton Trans.* **2015**, *44*, 12757−12770; (d) Martin-Diaconescu, V.; Gennari, M.; Gerey, B.; Tsui, E.; Kanady, J.; Tran, R.; Pecaut, J.; Maganas, D.; Krewald, V.; Goure, E.; Duboc, C.; Yano, J.; Agapie, T.; Collomb, M.-N.; DeBeer S. Ca K-Edge XAS as a Probe of Calcium Centers in Complex Systems. *Inorg. Chem.* **2015**, *54*, 1283−1292.

(30) (a) Macías, B.; Villa, M. V.; Lapresa, R.; Alzuet, G.; Hernández-Gil, J.; Sanz, F. Mn(II) Complexes with Sulfonamides as Ligands. DNA Interaction Studies and Nuclease Activity. *J. Inorg. Biochem.* **2012**, *115*, 64–71; (b) Seidler-Egdal, R. K.; Johansson, F. B.; Veltze, S.; Skou, E. M.; Bond, A. D.; McKenzie, C. J. Tunability of the $M^{II}M^{III}/M^{II}_2$ and $M^{III}_2/M^{II}M^{III}$ (M = Mn, Co) Couples in bis-μ-*O*,*O′*-Carboxylato-μ-OR Bridged Complexes. *Dalton Trans.* **2011**, *40*, 3336–3345; (c) Veltze, S.; Egdal, R. K.; Johansson, F. B.; Bond, A. D.; McKenzie, C. J. Coordinative Fexibility in an Acyclic Bis(sulfonamide) Ligand. *Dalton Trans.* **2009**, 10495–10504.

(31) Gao, J.; Ye, K.; He, M.; Xiong, W.-W.; Cao, W.; Lee, Z. Y.; Wang, Y.; Wu, T.; Huo, F.; Liu, X.; Zhang, Q. Tuning Metal–Carboxylate Coordination in Crystalline Metal–Organic Frameworks Through Surfactant Media. *J. Solid State Chem.* **2013**, *206*, 27–31.

(32) Drahos, B.; Kubicek, V.; Bonnet, C. S.; Hermann, P.; Lukes, I.; Toth, E. Dissociation Kinetics of Mn^{2+} Complexes of NOTA and DOTA. *Dalton Trans.* **2011**, *40*, 1945–1951.

(33) Van der Merwe, M. J.; Boeyens, J. C. A.; Hancock, R. D. Crystallographic and Thermodynamic Study of Metal Ion Size Selectivity in the Ligand 1,4,7-Triazacyclononane-*N*,*N*',*N*''-triacetate. *Inorg. Chem.* **1985**, *24*, 1208–1213.

(34) Pujales-Paradela, R.; Carniato, F.; Uzal-Varela, R.; Brandariz, I.; Iglesias, E.; Platas-Iglesias, C.; Botta, M.; Esteban-Gómez, D. A Pentadentate Member of the Picolinate Family for Mn(II) Complexation and an Amphiphilic Derivative. *Dalton Trans.* **2019**, *48*, 696–710.

(35) Takacs, A.; Napolitano, R.; Purgel, M.; Benyei, A. C.; Zekany, L.; Brucher, E.; Toth, I.; Baranyai, Z.; Aime, S. Solution Structures, Stabilities, Kinetics, and Dynamics of DO3A and DO3A−Sulphonamide Complexes. *Inorg. Chem.* **2014**, *53*, 2858–2872.

(36) Lowe, M. P.; Parker, D. pH Switched Sensitisation of Europium(III) by a Dansyl group. *Inorg. Chim. Acta* **2001**, *317*, 163-173.

(37) Rodríguez-Rodríguez, A.; Garda, Z.; Ruscsák, E.; Esteban-Gómez, D.; de Blas, A.; Rodríguez-Blas, T.; Lima, L. M. P.; Beyler, M.; Tripier, R.; Tircsó, G.; Platas-Iglesias, C. Stable Mn^{2+}, Cu^{2+} and Ln^{3+} Complexes with Cyclen-Based Ligands Functionalized with Picolinate Pendant Arms. *Dalton Trans.* **2015**, *44*, 5017–5031.

(38) V. Amendola, L. Fabbrizzi, L. Mosca, F.-P. Schmidtchen, Urea-, Squaramide-, and Sulfonamide-Based Anion Receptors: A Thermodynamic Study. *Chem. Eur. J.* **2011**, *17*, 5973-5981.

(39) Cortes, S.; Brucher, E.; Geraldes, C. F. G. C.; Sherry, A. D. Potentiometry and NMR Studies of l,5,9-Triazacyclododecane-N,N',N''-triacetic Acid and Its Metal Ion Complexes. *Inorg. Chem.* **1990**, *29*, 5–9.

(40) Drahos, B.; Kotek, J.; Hermann, P.; Lukes, I.; Toth, E. Mn^{2+} Complexes with Pyridine-Containing 15-Membered Macrocycles: Thermodynamic, Kinetic, Crystallographic, and $^1H/^{17}O$ Relaxation Studies. *Inorg. Chem.* **2010**, *49*, 3224–3238.

(41) Botta, M.; Carniato, F.; Esteban-Gómez, D.; Platas-Iglesias, C.; Tei, L. Mn(II) Compounds as an Alternative to Gd-Based MRI Probes. *Future Med. Chem.* **2019**, *11*, 1461–1483.

(42) Esteban-Gómez, D.; Cassino, C.; Botta, M.; Platas-Iglesias, C. ^{17}O and ^1H Relaxometric and DFT Study of Hyperfine Coupling Constants in $[Mn(H_2O)_6]^{2+}$. *RSC Adv.* **2014**, *4*, 7094–7103.

(43) Balogh, E.; He, Z.; Hsieh, W.; Liu, S.; Toth, E. Dinuclear Complexes Formed with the Triazacyclononane Derivative $ENOTA^{4-}$: High-Pressure ^{17}O NMR Evidence of an Associative Water Exchange on $[Mn^{II}_2(ENOTA)(H_2O)_2]$. *Inorg. Chem.* **2007**, *46*, 238-250.

(44) Aime, S.; Botta, M.; Esteban-Gómez, D.; Platas-Iglesias, C. Characterisation of Magnetic Resonance Imaging (MRI) Contrast Agents Using NMR Relaxometry. *Mol. Phys.* **2019**, *117*, 898–909.

(45) Freed, J. H. Dynamic Effects of Pair Correlation Functions on Spin Relaxation by Translational Diffusion in Liquids. II. Finite Jumps and Independent T_1 Processes. *J. Chem. Phys.* **1978**, *68*, 4034−4037.

(46) Mills, R. Self-Diffusion in Normal and Heavy Water in the Range 1-45°. *J. Phys. Chem.* **1973**, *77*, 685−688.

(47) Luz, Z.; Meiboom, S. Proton Relaxation in Dilute Solutions of Cobalt(II) and Nickel(II) Ions in Methanol and the Rate of Methanol Exchange of the Solvation Sphere. *J. Chem. Phys.* **1964**, *40*, 2686−2693.

(48) (a) Solomon, I. Relaxation Processes in a System of Two Spins. *Phys. Rev.* **1955**, *99*, 559−565; (b) Solomon, I.; Bloembergen, N. Nuclear Magnetic Interactions in the HF Molecule. *J. Chem. Phys.* **1956**, *25*, 261−266; (c) Bloembergen, N. Proton Relaxation Times in Paramagnetic Solutions. *J. Chem. Phys.* **1957**, *27*, 572−573; (d) Bloembergen, N.; Morgan, L. O. Proton Relaxation Times in Paramagnetic Solutions. Effects of Electron Spin Relaxation *J. Chem. Phys.* **1961**, *34*, 842−850.

(49) Gale, E. M.; Zhu, J.; Caravan, P. Direct Measurement of the Mn(II) Hydration State in Metal Complexes and Metalloproteins through ^{17}O NMR Line Widths. *J. Am. Chem. Soc.* **2013**, *135*, 18600−18608.

(50) (a) Borel, A.; Kang, H.; Gateau, C.; Mazzanti, M.; Clarkson, R. B.; Belford, R. L. Variable Temperature and EPR Frequency Study of Two Aqueous Gd(III) Complexes with Unprecedented Sharp Lines. *J. Phys. Chem. A* **2006**, *110*, 12434–12438; (b) Borel, A.; Laus, S.; Ozarowski, A.; Gateau, C.; Nonat, A.; Mazzanti, M.; Helm, L. Multiple-Frequency EPR Spectra of Two Aqueous Gd^{3+} Polyamino Polypyridine Carboxylate Complexes: A Study of High Field Effects. *J. Phys. Chem. A* **2007**, *111*, 5399–5407; (c) Khan, S.; Kubica-Misztal, A.; Kruk, D.; Kowalewski, J.; Odelius, M. Systematic Theoretical Investigation of the Zero-Field Splitting in

Gd(III) Complexes: Wave Function and Density Functional Approaches. *J. Chem. Phys.* **2015**, *142*, 034304.

(51) Fornasier, R.; Milani, D.; Scrimin, P.; Tonellato, U. Functional Micellar Catalysis. Part 8. Catalysis of the Hydrolysis of *p*-Nitrophenyl Picolinate by Metal-Chelating Micelles Containing Copper(II) or Zinc(II). *J. Chem. Soc. Perkin Trans. 2* **1986**, 233–237.

(52) Tan, J.; Tang, W.; Sun, Y.; Jiang, Z.; Chen, F.; Xu, L.; Fan, Q.; Xiao, J. pH-Regulated Transfer Hydrogenation of Quinoxalines with a Cp*Ir-diamine Catalyst in Aqueous Media. *Tetrahedron* **2011**, *67*, 6206–6213.

(53) Moss, T. A.; Barber, D. M.; Kyle, A. F.; Doxon, D. J. Catalytic Asymmetric Alkylation Reactions for the Construction of Protected Ethylene-Amino and Propylene-Amino Motifs Attached to Quaternary Sterocenters. *Chem. Eur. J.* **2013**, *19*, 3071–3081.

(54) Gans, P.; Sabatini, A.; Vacca, A. Investigation of Equilibria in Solution. Determination of Equilibrium Constants with the HYPERQUAD Suite of Programs. *Talanta* **1996**, *43*, 1739−1753.

(55) Vogel, A. I. Vogel's Textbook of Quantitative Chemical Analysis. Harlow, Essex, England: New York: Longman Scientific & Technical; Wiley, 1989.

(56) Caneda-Martínez, L.; Valencia, L.; Fernández-Pérez, I.; Regueiro-Figueroa, M.; Angelovski, G.; Brandariz, I.; Esteban-Gómez, D.; Platas-Iglesias, C. Toward Inert Paramagnetic Ni(II)-Based Chemical Exchange Saturation Transfer MRI Agents. *Dalton Trans.* **2017**, *46*, 15095–15106.

(57) Bates, R.G.: Determination of pH, Theory and Practice. 2nd Edition, John Wiley & Sons, New York, London, Sydney, Toronto, 1973.

(58) (a) Evans, D. F. The Determination of the Paramagnetic Susceptibility of Substances in Solution by Nuclear Magnetic Resonance *J. Chem. Soc.* **1959**, 2003-2005; (b) Evans, D. F.; Fazakerley, G. V.; Phillips, R. F. Organometallic Compounds of Bivalent Europium, Ytterbium, and Samarium. *J. Chem. Soc. A* **1971**, 1931-1934.

(59) Bruker, APEX2, SMART, SAINT, Bruker AXS Inc., Madison, Wisconsin, USA, 2007.

(60) SAINT Version 8.37A (Bruker AXS Inc., 2015).

(61) SADABS Version 2014/5 (Sheldrick, Bruker AXS Inc.).

(62) SHELXT Version 2014/5. Sheldrick, G. M. SHELXT - Integrated Space-Group and Crystal-Structure Determination. *Acta Cryst.* **2015**, *A71*, 3–8.

(63) SHELXL Version 2018/3. Sheldrick, G. M. A Short History of SHELX. *Acta Cryst.* **2008**, *A64*, 112–122.